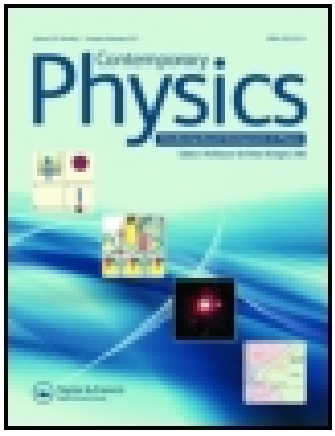

Contemporary Physics

Publication details, including instructions for authors and subscription information:
http://www.tandfonline.com/loi/tcph20

Single particle sources and quantum heat fluctuations

F. Battista[a]

[a] Departamento de Fisica, FCEyN, Universidad de Buenos Aires and IFIBA, Buenos Aires, Argentina.

Published online: 10 Jul 2014.

Contemporary Physics, 2014
http://dx.doi.org/10.1080/00107514.2014.934528

Taylor & Francis
Taylor & Francis Group

Single particle sources and quantum heat fluctuations

F. Battista*

Departamento de Fisica, FCEyN, Universidad de Buenos Aires and IFIBA, Buenos Aires, Argentina

(*Received 14 April 2014; accepted 10 June 2014*)

The miniaturisation of electronic devices has been a well-known trend in engineering over almost 50 years. The technological advancement in the field can now provide an astonishing control of charge transport in mesoscopic structures. Single particle pumping, namely the control in time and space of the flow of an arbitrarily small number of electrons or holes, has been realised in various kind of structure with, in some cases, very high accuracies. The first half of the manuscript provides a brief overview of different experimental realisations of single particle sources. Though these devices allow to minimise charge fluctuations in the charge current, because of Heisenberg's uncertainty principle, the emitted particles are characterised by energy fluctuations. The consequences of it are of great relevance and presented in the second part of the paper.

Keywords: single particle sources; quantised current; quantum heat fluctuations

1. Introduction to single particle sources

The continuing miniaturisation of electronic devices has now reached the mesoscopic scale.

Mesoscopic scale devices [1,2] are constituted by large number of atoms but they are ruled by quantum mechanics. Using mesoscopic systems, the dual nature of the electrons [3] can be exploited in order to reach new kinds of technology.

Single particle sources (SPSs) are one kind of mesoscopic devices. While a macroscopic electrical current is perceived as a continuous quantity and it is given by a large, uncontrolled number of propagating electrons characterised by large fluctuations, a SPS can induce current pulses given by a controlled number of electrons or holes during a desired time interval, in a desired area of a circuit and characterised by very low fluctuations. The main applications of SPSs are in the fields of metrology and quantum information.

The first theoretical investigation of the possibility to achieve quantised charge transfer using the quantum properties of particles was performed by Thouless [4] in the early '80s and it concerned adiabatic pumping, i.e. the particles spend inside the SPS a time shorter than the time scale over which the particles are emitted. The idea of quantised currents was later extended to mesoscopic systems using a scattering approach [5,6].

Single particle sources are generally driven periodically in time. During each pumping period $\mathcal{T}$, a number of particles is emitted. The quantised current they produce is given by an integer number n of electrons (holes) times the frequency f at which they are injected $I = +(-)nef$ (e is the electron charge). The number of pumped particles n can fluctuate due to failures in the pumping mechanisms: more or fewer than the desired number of particles per period can be transmitted. An experimental measure of these fluctuations is given by the zero frequency current correlator (or noise) [7]. When the zero frequency current correlator is zero, the source works in an ideal way, exactly the same number of particles is emitted during each period, (Figure 1(a)) and the accuracy is maximal. If the number n changes every period, i.e. it fluctuates around an average value, the pump is less accurate and it is characterised by a finite zero frequency current correlator (Figure 1(b)).

A big effort has been made to reduce these fluctuations, achieving very good emission accuracy [8].

Electrons (or holes) are not only charge carriers but also energy carriers. Important for applications and relevant in fundamental studies is the investigation of energy transport properties in mesoscopic systems. For instance, the injection of single electrons from SPSs into a system leads to very different physics compared to injection from a reservoir kept at constant bias. The electrons emitted by a biased reservoir (electrode) can be described by plane waves energy distributed according to $f(E)$, the Fermi-Dirac distribution. If the electron injection is performed by means of an SPS, however, the scenario is altered. According to Heisenberg's uncertainty principle [3], a particle emitted during

*Email: battista@df.uba.ar

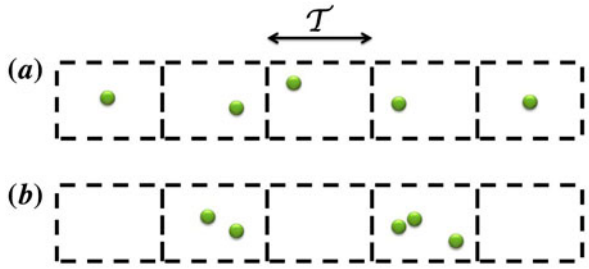

Figure 1. Pictorial representation of 'noise' characterising a SPS. At each period of length $\mathcal{T}$ (sketched as a dashed box), the source is expected to pump on average a given number of particle. When this number is exactly the same for every period, the signal is characterised by zero noise (*a*). However, in experimental realisations, this number changes for every period, preserving the average number of pumped particles per period, but giving a noisy signal (*b*).

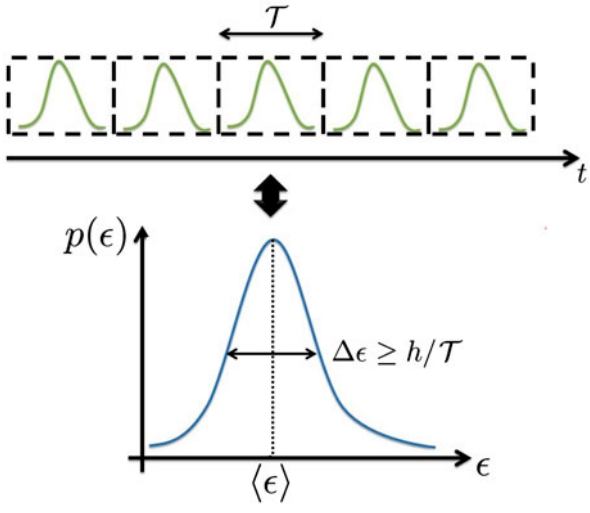

Figure 2. Pictorial representation of the Heisenberg's uncertainty principle. A particle emitted during a time interval $\mathcal{T}$, the pumping period of a SPS, has an uncertainty in energy larger than $h/\mathcal{T}$.

the time interval $\mathcal{T}$ has an uncertainty in energy larger than $h/\mathcal{T}$ (Figure 2). As a consequence, in case of emission from ideal sources even if the stream of electrons does not display any low-frequency charge noise, the energy, or heat, carried by the electrons fluctuates [9]. The uncertainty in the energy of the emitted particles affects the thermoelectric properties of the system, which can have a significant impact on nanoelectronic devices. Coherent on-demand sources can be used to investigate the statistics of temperature [10,11], to study heat transfer [12,13] fluctuations in mesoscopic systems or to test heat fluctuation relations [14–17] in the quantum regime [18].

The manuscript is divided in Part I and Part II. Part I is an introduction to single particles sources and it has the purpose to illustrate in a simple way the experimental achievements in this field. It includes Section 2 and Section 3. Section 2 focuses on the main applications of SPSs, in order to provide the reader with a better understanding of the motivations pushing forward the technological evolution of SPS realisation and the need for further studies on the energy transport properties related to SPS implementation in bigger circuits. Section 3 gives a brief overview of the oldest and newest experimental implementations of SPSs.

Part II focuses on the thermal aspects of the injection of single wave packets into a circuit. We warn the reader that this part, due to the nature of the topic, is more technical, showing more equations. It includes Section 4 and Section 5. In Section 4, the general spectral distribution of a pumped particle is introduced and some examples of experimental measurements are described. Section 5 illustrates how the injection of such particles affects the thermoelectric properties of a larger circuit. Conclusions are in Section 6. In the table below we provide a list of acronyms used throughout the text.

Acronym	
SPS	single particle sources
2DEG	two-dimensional electron gas
QPC	quantum point contact
QD	quantum dot
SAW	surface acoustic wave
DC	direct current
AC	alternating current
FCS	full counting statistics
RC	resistor-capacitor

PART I

2. Applications

Time-controlled charge transport allows, on one hand, the study of fundamental properties as coherence [19], correlations [20–22] and interactions [23] of electrons and holes. On the other hand, the main applications of single particles sources are in two different fields: metrology and quantum information.

2.1. Metrology

Metrology is the science of measurement and the study of the definition of fundamental measurement units. Already J. C. Maxwell in the late nineteenth century proposed to define the units of measure in terms of universal constants as the electron charge e or the Planck's constant h. In the last decades, quantum mechanics has been playing an important role in this respect. For instance, concerning charge transport, the unit Volt can be defined in terms of fundamental units e and h using the Josephson effect [24]. Between the wave functions of the two superconducting electrodes constituting a Josephson junction, there is a phase difference.

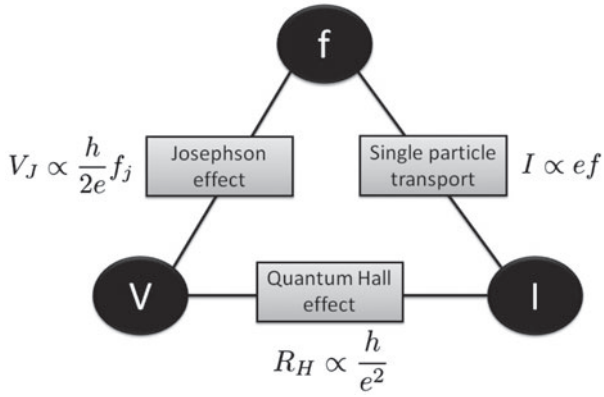

Figure 3. The metrological triangle. The units Volt, Ohm and Ampere can be expressed in terms of universal constants using quantum effects: Josephson effect, quantum Hall effect and single particle pumping, respectively.

Using an high-frequency signal f_j, this phase difference can be fixed. The consequence is a quantisation of the voltage across the junction $V = n_j \frac{h}{2e} f_j$ where n_j is an integer number. Thus the Volt can be expressed in units of $h/2e$. Similarly, the Ohm can be redefined using the quantum Hall effect (which was first observed by von Klitzing et al. [25]). At low temperatures, a two-dimensional electron gas (2DEG) subjected to strong perpendicular magnetic fields shows a Hall resistance which is quantised in units of h/e^2. While these new definitions of Volt and Ohm are widely used by experimentalists, there is yet no counterpart for the Ampere.

The SPSs could be used to close the so-called metrological triangle (Figure 3), a pictorial way to describe the relation between Volt, Ohm and Ampere.

Indeed, the Ampere could be redefined in terms of a number of electrons crossing a section of a conductor at a given frequency. The definition could be tested against Voltage and Resistance via Ohm's law for a consistency check of the fundamental constants of nature h and e. In this instance, the granularity of the electric charge, i.e. its quantisation, or in other words the particle nature of electrons is crucial. To be able to perform such a test, this kind of applications requires a very high accuracy in particle emission. In order to be consistent with the accuracy at which the electrical charge e is known and to improve on the accuracy with which the Ampere is already defined, a SPS suitable for metrological purposes has to induce current pulses I at a frequency in the range of GHz and characterised by fluctuations δI of the order $\sim 10^{-7} I$ [8].

2.2. *Quantum information*

The manipulation of single particles is important for quantum computing too. Any quantum information protocol needs an internal clock to control operations in time or to time different signals. Furthermore, the developments in quantum electron optics give now the possibility to entangle two electrons and separate them later [26], thus connecting quantum electron optics with quantum information processing in solid state systems.

In quantum electron optics, the wave character of particles is exploited. In this field, mesoscopic devices are designed to realise the fermionic analogues of optical experiments, as interferometry experiments. One of the earlier realisations of an electronic interferometer was based on the Aharonov–Bohm effect, the Aharonov–Bohm ring [27]. Other geometries have been mimicked in solid state systems, such as the Mach–Zender interferometer [28] or the analogue of the photonic Hanbury–Brown–Twiss experiment, which demonstrated the bosonic nature of photons through correlation measurements. In case of electrons it showed the fermionic nature of these particles, see for example the experiment in [29].

These setups are realised with 2DEGs subjected to a strong perpendicular magnetic field in order to reach the quantum Hall regime. In this regime transport takes place along the, so-called, edge states and it is thus unidirectional. A charged particle in a strong magnetic field has a circular orbit of radius r_c (cyclotron radius). But if the distance of the particle from the edge of the device is smaller than r_c then the particle will bounce against the edge not reversing its direction of motion. It will thus propagate from one side to the other of the device (Figure 4(a)). These delocalised states available for transport are the edge states. Even in presence of inelastic or elastic scattering, for example against an impurity, the carriers moving along the edge states cannot reverse their motion [30]. This holds if (a) the impurity potential varies smoothly along the cyclotron radius but its range is small compared to the sample and (b) the mean distance between the impurities is larger than the cyclotron radius. Similarly, the inelastic scattering length must exceed the cyclotron radius length. Thus the edge states, despite elastic or inelastic scattering, are transport channels just as those in an ideal conductor at zero magnetic field. Transport is unidirectional and coherent.

For the implementation of optic interferometers, it is important also to have a beam splitter. In quantum electron optics, this role is played by a quantum point contact (QPC) sketched in Figure 4(b). A QPC is created by a gate capacitively coupled with a 2DEG. By tuning the voltage applied to the gate, an electronic potential is induced on the underlying 2DEG allowing particles to propagate along the same edge state with a probability T or to be scattered to the counter-propagating edge state with probability $R = 1 - T$.

The detailed description of experimental realisations of the above-mentioned electronic interferometers realised in solid state systems goes beyond the purposes of this review, but the reader is invited to find out more about this interesting emerging field in [31] and references therein.

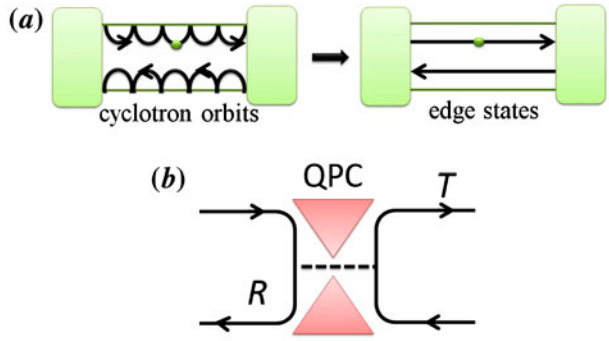

Figure 4. (*a*) Sketch of propagation of a charged particle in a 2DEG subjected to a perpendicular magnetic field. Classically, the electrons have cyclotron orbits. If the distance from the edges is smaller than the radius of the orbits, the electron propagates from one side to the other of the sample 'bumping' against the transversal confinement. This corresponds to the quantum edge state, the only state available to transport (black arrow). The transport is then unidirectional. (*b*) Sketch of a QPC acting as a beam splitter. A particle propagating along an edge state (black arrow) can be reflected with probability R or transmitted with probability T across the QPC.

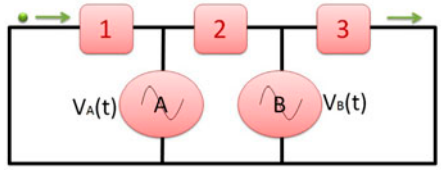

Figure 5. Circuit representation of the pump in [33]. No bias is applied. There are three junctions 1, 2, 3 (squares). The voltages $V_A(t)$ and $V_B(t)$ applied to the gates (sketched as circles) are time-periodic voltages , $\pi/2$ out of phase. The driving of the gates controls in a periodic way the tunnelling of the electrons from and to the external leads and between the junctions.

3. Pumping overview

There are several possible realisations of SPSs which will here be grouped in two main types: pumps and turnstiles. In the case of pump devices, the direction of the electron transfer is determined by the phase relationship between two parameters and it is thus reversible when changing the phase difference. In the case of turnstiles, a source-drain bias is applied and the direction of the electron transfer is imposed by the voltage drop across the whole structure. In the following, we will show some examples of both kinds.

3.1. Early works: examples

3.1.1. Metallic devices

Metrology motivated the first realisations of SPSs. They consisted of metallic quantum dots (QDs) and worked in the Coulomb blockade regime [32,33]. Phase coherence was not required. For example, Pothier et al. [33] realised a pump composed by three Al/Al_2O_3 tunnel junctions 1, 2, 3 with capacitances C_1, C_2 and C_3 and two gates A, B with capacitances C_A and C_B. The gates had smaller capacitances than the junctions, i.e. $C_A, C_B \ll C_1, C_2, C_3$. The gate A was between the first island 1 and the middle one 2, the gate B was between junctions 2 and 3 (the corresponding circuit is shown in Figure 5). No bias was applied on the two external leads. In the first part of the pumping cycle particles did not tunnel into any of the islands due to the Coulomb blockade effect (the energy cost of adding an extra electron inside any of the QDs was too high). Two time-periodic voltages $V_A(t)$ and $V_B(t)$ were applied to the gates with a phase shift of $\phi = \pi/2$. The voltage $V_A(t)$ made the tunnelling from 1 to 2 energetically favourable. Once the particle was in the central junction 2, the second gate voltage $V_B(t)$ made favourable the tunnelling from junction 2 to junction 3. At the end of the cycle, an electron was transmitted from one side of the device to the other without any potential drop between the two sides. With a phase shift between $V_A(t)$ and $V_B(t)$ of $\phi = 3\pi/2$, the direction of the transfer would have been from junction 3 to 1. In order to avoid uncontrolled cotunnelling events, the tunnelling probability was kept very small and this limited the pumping frequency to the MHz regime. Therefore, metallic devices based on Coulomb blockade effect are questionable for metrological purposes.

One of the most recent metallic pump was realised by Camarota et al. [34]. They reduced cotunnelling and photon-assisted tunnelling, another mechanism limiting the accuracy of the source, thanks to a dissipative environment reaching the best accuracy known for these kind of metallic devices [34].

3.1.2. Semiconductor devices

Coulomb blockade effects were also of key importance in the experimental realisation of the first semiconductor turnstile by Kouwenhoven et al. [35]. The turnstile consisted of a semiconductor QD defined by two QPCs realised by means of electrostatic gates on the top of a 2DEG. The direction of the pumping of the electrons was given by the applied voltage eV (Figure 6). The voltages defining the QPCs were periodic in time with frequency f and π-shifted in phase. At the beginning of the pumping cycle (Figure 6(*a*)), the dot was populated by N electrons and the high barrier prevented one more electron from tunnelling into the dot. When the potential of left barrier was decreased (Figure 6(*b*)), electrons had a higher probability to tunnel inside the dot from the left lead and the QD charging level $N + 1$ could be populated. The right barrier was then increased in order to suppressed the tunnelling out to the right lead trapping the electron in the dot (Figure 6(*c*)). The Coulomb blockade effect limited the number of tunnelling electrons to 1 as the charge state $N+2$ was not within the bias window. During the last step of the cycle (Figure 6(*d*)), the left barrier

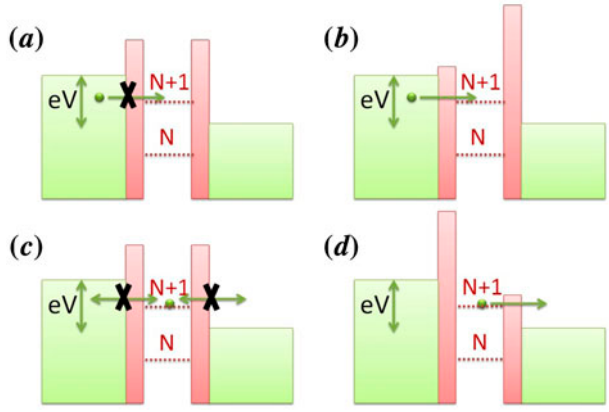

Figure 6. Representation of the four steps of the pumping cycle of the turnstile of [35]. A quantum dot is coupled to two leads through two tunnelling barriers. A bias eV is applied between the two external leads giving the direction of electron transfer. When the barrier is tuned to be higher, the tunnelling in and out of the dot is inhibited (crossed arrow). When the barrier is lowered down, the tunnelling is enhanced (see text). The driving of the barriers is time periodic. This allows pumping of electrons from the left side to the right side in a controlled manner.

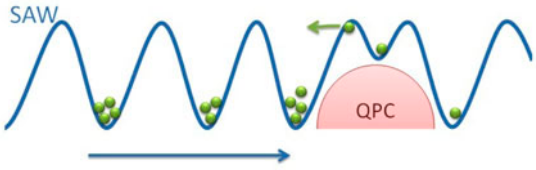

Figure 7. Sketch of the pumping mechanism of the SPS based on SAWs of [37]. The local minima of a SAW can be seen as propagating quantum dots, carrying several charges from the lead to the QPC. At the QPC, the same electrons are backscattered. This mechanism determines the number of electrons transmitted per cycle.

was increased and the right one was decreased releasing the electron trapped in the quantum dot in the right lead. Increasing the applied bias eV, m charge states could be found within the bias window, so m electrons could cross the dot at each period. As in the case of a metallic pump, the pumping frequency was in the MHz regime. A quite broad study of error mechanism that can arise in semiconductor devices and a comparison with metallic devices is in [36].

3.2. *Recent developments: examples*

We now continue with more recent realisations of SPSs. Some of them reached a pumping frequency of the order of GHz, needed for metrological applications [8].

3.2.1. *Surface acoustic waves devices*

Another way to pump particles from one side to the other of a device without applying a bias drop is to use surface acoustic waves (SAWs). Shilton et al. [37] realised it sending a SAW on a piezoelectric material. The local minima of this travelling potential can be seen as moving quantum dots, carrying several charges. These charges were thus brought from the lead to a constriction (QPC). The combination of the moving potential (SAW) and of the QPC potential determined the number of electrons transmitted from one side to the other of the device (Figure 7). In fact, tuning the steepness of the QPC potential reduced the number of electrons that could cross the constriction. On the top of this, the Coulomb charging energy made each local minimum of the surface acoustic wave populated by one electron. They reported a SAW frequency of 3 GHz. This experiment has been widely investigated theoretically [38–42] finding good agreement between theory and experiments. If on one hand these devices cannot have very good accuracy due to pumping errors difficult to avoid, on the other hand SAWs have been recently used as quantum buses between two dots with very good efficiency in emission and detection [43,44], useful for possible implementations of quantum information protocols in solid state systems.

3.2.2. *Hybrid structure devices*

Pekola et al. [45] developed a metallic hybrid normal-superconducting turnstile. A superconducting island was coupled with two normal metallic leads biased with eV. The superconducting island had an energy density of states with a gap Δ. In the perfect working condition $eV = \Delta$, the transfer of a single electron per period was guaranteed by the gap and by the Coulomb blockade effect (Figure 8). In fact on the top of the superconducting island there was a gate with a periodic applied bias $V_g(t)$. The dot was populated only when $V_g(t)$ was such that the electron could tunnel from the lead to the island finding a non-zero density of state. The Coulomb blockade prevented other electrons

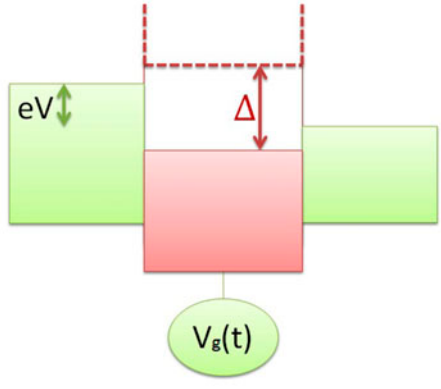

Figure 8. Scheme of the band structure of the hybrid structure used in [45]. Only when the voltage applied between the two leads equals the superconductor band gap $V_g = \Delta$ an electron finds available states (dashed boxed area) to tunnel across the superconducting island to the normal metallic electrode on the other side.

from tunnelling in. The dot discharged when $V_g(t)$ was such that the tunnelling out was energetically favourable. They reported a working frequency of 100 MHz and the accuracy was improved in a later experiment [46]. These devices can work in parallel [47] making them a promising source of accurate nanoampere currents, suitable for metrological purposes.

3.2.3. *Semiconductor nanowires devices*

Blumenthal et al. [48] realised a pump reaching the GHz pumping frequency.

The device was given by an etched GaAs/AlGaAs nanowire. On the top of it, capacitively coupled, there were three gate fingers (Figure 9(*a*)). No bias was applied across the structure. The leftmost and the rightmost gates were subjected to $V_L(t)$ and $V_R(t)$, respectively. The two potentials defined two barriers creating, together with the transversal confinement due to the nanowire, a quantum dot. The central finger was biased and determined the bottom potential of the QD when decoupled from the 2DEG. The gates were close enough to each other so that the electrons in the dot were subjected to an effective potential $V_{eff}(x,t)$ given by

$$V_{eff}(x,t) = a_L(x)V_L(t) + a_C(x)V_C + a_R(x)V_R(t). \quad (1)$$

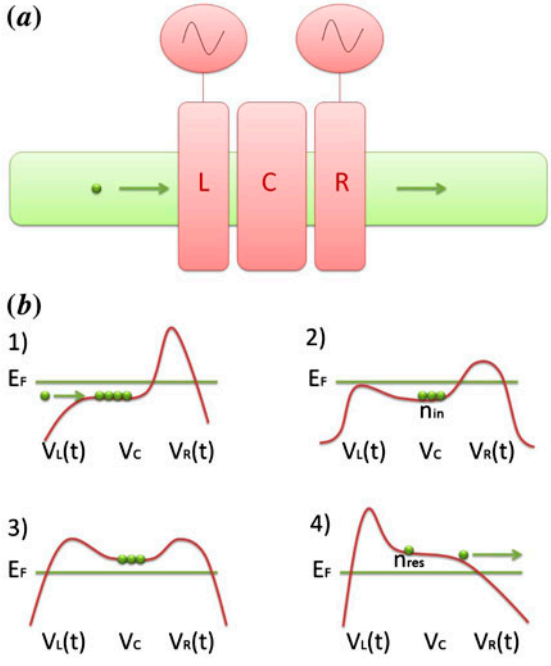

Figure 9. (*a*) Representation of the setup used in [48]. On the top of a quantum wire there are three gates. The three voltages $V_L(t)$, $V_R(t)$ and V_C applied to the gates design the potential experienced by electrons propagating in the wire. (*b*) Sketch of the evolution of the longitudinal potential over one pumping period. The pumping cycle is given by four steps: (1) lowering $V_L(t)$ allows the electrons to tunnel into the dot, (2) $V_L(t)$ increases trapping the electrons in the dot, (3) $V_R(t)$ is decreased, (4) the electrons are released from the dot to the right side.

The voltages $V_L(t)$ and $V_R(t)$ were modulated sinusoidally in time with a π shift. At the first step of the pumping cycle (Figure 9(*b*1)) $a_L(x)V_L(t)$ and $a_C(x)V_C$ were below the Fermi level while $a_R(x)V_R(t)$ was above so n_{in} electrons entered the dot. In step 2 (Figure 9(*b*2)), the voltage $V_L(t)$ was increased trapping the electrons in the dot and lifting them above the Fermi sea in the wire (Figure 9(*b*3)). In the fourth step of the cycle (Figure 9(*b*4)), $V_R(t)$ decreased and the dot was discharged, with only n_{res} electrons left in the dot. The pumped current I was thus:

$$I = -ef(n_{in} - n_{res}), \quad (2)$$

with f the pumping frequency. The average values of n_{in} and n_{res} were determined by the charging energy and their fluctuations were minimised tuning $V_{eff}(x,t)$. Single-parameter pumping has been realised with the same setup by Kaestner et al. [49]. In that case V_R was time-independent. When pumping $V_L(t)$, V_C was following along due to a capacitive coupling. Good pumping was achieved at $f =$ 80 MHz, but transport was blocked at GHz frequency. A similar experiment has been independently realised by Fujiwara group [50]. When a perpendicular magnetic field was applied, it was possible to achieve a better current quantisation [51,52]. The best accuracy for these systems has been reached by Giblin et al. [53].

3.2.4. *Atoms based devices*

Another kind of confined structure used to perform particles pumping in solid state systems are atoms [54–56]. One of the last achievements was a two-atom electron pump [57]. After doping with phosphorus atoms a silicon wire Roche et al. addressed only two atoms using three gates, left, right and a gate below the substrate (back gate). The part of the wire covered by the gates was depleted and characterised by a low concentrations of dopant. The other two sides constituted the source and the drain. The back gate was used to tune the coupling between the dopant atoms and the leads (Figure 10).

The left and right gates controlled the energy spectrum of the two atoms addressing each of them individually. Applying periodic signals to the side gates the energy configuration was changed in time in order to favour the tunnelling of electrons always in the desired direction similarly to what done with the metallic islands in [33]. The device worked at low pumping frequencies f, losing optimal pumping properties when reaching $f = 10$ MHz.

3.2.5. *Pumping in the quantum Hall regime*

Coherent pumping in the quantum Hall regime, as already explained, is a key ingredient of quantum electron optics, and therefore for any of its applications in quantum information protocols. One of the most popular experimental achievements in this field is the AC pump realised by Fève

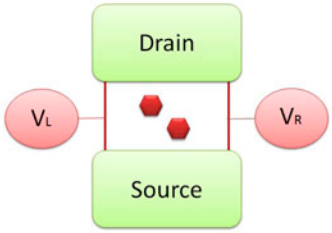

Figure 10. Scheme of the pump realised in [57]. A silicon wire is doped with phosphorus atoms (hexagons in the centre). Thanks to a back gate (not sketched) a region is depleted and only two atoms are addressed by two side gates V_L and V_R. Tuning the energy spectrum of the two atoms in a controlled manner electron tunnelling from source to drain can be controlled.

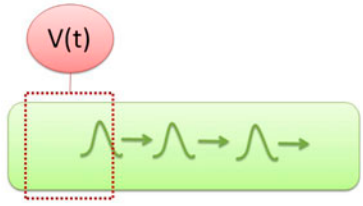

Figure 12. Pictorial representation of Leviton excitations above the Fermi sea. A specific voltage pulse proposed in [64] is applied to a conductor (dashed box). It originates Lorentzian current pulses given only by electron-like excitations of the Fermi sea. The corresponding hole-like excitations (not sketched) propagates in opposite direction.

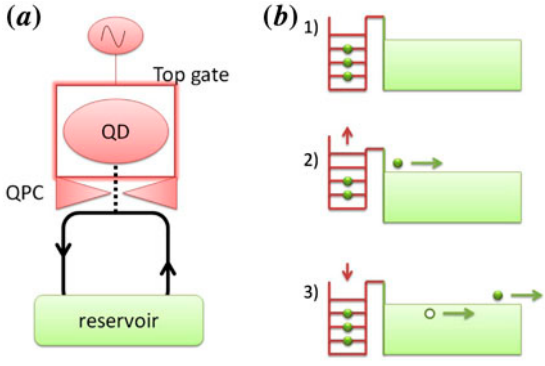

Figure 11. (*a*) Scheme of the on-demand single electron source of [58]. A quantum dot is coupled to a 2DEG reservoir through a QPC. Transport takes place along an edge state (black arrow). The QD has a top gate subjected to an oscillating time-periodic voltage with a capacitance making the quantum dot charging energy negligible. (*b*) Scheme of the pumping principle: the resonance of the QD is shifted above and below the 2DEG reservoir due to the applied top-gate voltage. As a consequence an electron and an hole are alternatively emitted into the reservoir.

et al. [58]. A quantum dot was coupled through a quantum point contact to a spin polarised edge state induced in a two-dimensional electron gas by a strong perpendicular magnetic field (Figure 11(*a*)). The QD is a component of a mesoscopic capacitor. On the top of it, in fact, there is an electrode. The top-gate capacitance was so large that the charging effects were negligible. A time periodic voltage was applied to the QD top electrode. As a main effect, the QD resonance moved above and below the Fermi level E_F of the reservoir coupled with the edge state, as shown in Figure 11(*b*). When the resonance was below E_F, the electron carried from the reservoir by the edge state could tunnel into the dot and charged it. This left a hole propagating towards the reservoir. Then the electron was emitted by the QD into the edge channel when the resonance was pushed above E_F. The electron, propagating along the edge state, reached the reservoir. An alternate current (alternate emission of hole and electron) was thus pumped. This cycle could be run at GHz frequencies.

For quantum information purposes, it would be desirable an on-demand source that separates the stream of electrons from the stream of holes as the turnstile proposed in [59].

During another experiment on the same setup Mahé et al. [20] measuring the current correlators detected two kinds of quantum noise: the shot noise and, what they called, quantum jitter. While the fluctuations of the number of electron emitted per period give the shot noise, the quantum jitter is given by the uncertainty in the tunnelling escape time, the time the electrons take to escape from the QD through the QPC. At optimal working conditions, the shot noise is basically suppressed and only the quantum jitter effect remains. Such an on-demand source has been largely studied [60–62] and integrated in more complicated setups [29,63].

3.2.6. *Latest achievement: the Leviton*

A way of performing electron pumping not relying on quantum confinements has been proposed by Levitov and coworkers [64]. When applying a time-dependent voltage pulse $V(t)$ on a conductor, several excitations of the Fermi sea are created. The many-body state created is given by electron and hole excitations above and below the Fermi energy E_F. Under a specific choice of $V(t)$ it is possible to excite only electron-like excitations from a Fermi sea, free from hole-like excitations [65]. Such a pulse should have a Lorentzian shape giving, integrated over time, an integer number l, $\int dteV(t)/h = l$. These kind of pulses lead to minimum of the zero frequency current correlator, confirming the absence of hole excitations. In the experimental work performed by Dubois et al. [66], particles excited above the Fermi sea in this way were named Levitons. In that experiment periodic Lorentzian pulses were applied on a two-terminal conductor (Figure 12). These very peculiar electronic excitations propagate coherently. The creation of a Leviton probably is the simplest, but not the most trivial,

way of pumping particles. It has a wide range of possible applications being easy to integrate in several setups.

PART II

4. Electrons are energy carriers

Complete information about the state emitted by a single particle source, including the spectral profile, can be obtained from the calculation of the full many-body wave function. Such a calculation is performed in [64] to calculate the wave function of a Leviton. In [67], it was further shown that the same kind of wave packet characterised the electrons emitted by the pump in the Fève et al. [58] experiment when the quantum dot energy level is linearly driven in time across the Fermi sea. A simpler approach is instead taken in [68] to calculate wave functions of an electron emitted by a turnstile in the quantum Hall regime [59]. The model can be extended to any of the setup based on confined structures where the particle is emitted well above the unperturbed Fermi sea as for example the mesoscopic capacitor used in [58] driven in the non-adiabatic regime or the pump in [69]. Ferraro et al. showed that the Wigner functions of the emitted electrons can be used to derived the same energy wave packet [70].

We consider the ideal case of a source emitting one electron above the Fermi sea of a conductor and leaving the Fermi sea unperturbed. The electron wave packet in second quantisation reads

$$|\psi\rangle = \int_0^\infty c_\epsilon b_\epsilon^\dagger |0\rangle \, d\epsilon \tag{3}$$

where $b_\epsilon^\dagger$ is the creation operator for an electron emitted at energy $\epsilon > 0$ above the Fermi sea. The state $|0\rangle$ is the unperturbed Fermi sea. The energy distribution of the emitted electron $p(\epsilon)$ is given by the coefficients c_ϵ, $p(\epsilon) = |c_\epsilon|^2$, and $\int_0^\infty p(\epsilon)d\epsilon = 1$. The average value of the distribution, i.e. the average energy of an electron emitted during one period, is

$$\langle\epsilon\rangle = \int_0^\infty \epsilon |c_\epsilon|^2 d\epsilon, \tag{4}$$

with its standard deviation, namely the wave-packet width, given by $\Delta\epsilon = \sqrt{\langle\epsilon^2\rangle - \langle\epsilon\rangle^2}$ where

$$\langle\epsilon^2\rangle = \int_0^\infty \epsilon^2 |c_\epsilon|^2 d\epsilon. \tag{5}$$

4.1. Measurements of out of equilibrium energy distributions

Measuring the energy distribution of a pumped electron in experiments is rather complicated. Due to the chiral properties of transport along edges states some techniques have been developed in the quantum Hall regime for testing the energy distribution of out of equilibrium excitations of the Fermi sea.

Fletcher et al. [69] developed a time resolved spectroscopy technique able to detect the energy distribution of the emitted electron and the time of arrival at the detector. They used the source of [48] based on two top gates defining a quantum dot in a wire in the quantum Hall regime. Tuning the voltage applied on the gate a particle was lifted from the Fermi sea, trapped in the quantum dot and released at a very high energy, well above thermal excitations. After propagating along the edge states for few micrometer it was scattered by a gate barrier acting as an energy filter. Measuring the transmitted current at different barrier gate potential allowed to recover the energy wave-packet profile. The same measurement, but with a time-dependent signal applied to the barrier gate gave information on the arrival time of the wave packet.

Bocquillon et al. [29] exploited interferometry effects to measure the energy distribution of electrons emitted by the Fève's pump [58]. They realised the electronic analogue of the Hanbury–Brown and Twiss experiment. The particles emitted by the SPS were propagating along edge states towards a QPC and thus they were parted into two streams, the transmitted and the reflected one. They measured the correlations between the two originated currents. The correlator was suppressed due to the antibunching between the electrons pumped by the SPS at low energy and the electrons thermally excited from the Fermi sea. This suppression was used as a probe of the pumped electrons energy distribution. Other ways of detecting the energy emission for individual electrons are available such as charge counting in weakly tunnel coupled systems [12,15,17].

An important tool for investigations of out of equilibrium distributions of edge state in a more direct way was achieved by Altimiras et al. [71]. A single level in a quantum dot was weakly coupled to an edge state and it acted as an energy filter. Measuring the current emitted by the dot allowed the reconstruction of the energy distribution of the electrons entering the dot and thus of the edge state. The energy dissipation taking place along edge states of a few hundreds of nanometres length was found to be negligible. This gives strength to the analogy done in quantum electron optics between the electron transport in the quantum Hall regime in nanostructures and light rays in quantum optics. In later experiments, where the edge states were few micrometers long the energy relaxation was not any more negligible [72], but techniques to suppress it have been realised and presented in [72,73]. We highlight to the reader that the modification of the spectral properties of the particles propagating along the edge is a sensitive tool for investigating electronic interactions [74–76]. Even if the experiment in [71] does not measure the energy distribution of pumped electrons propagating along edge states, a SPS could be easily integrated in the setup [68].

Other successful experiments measuring heat current in integer or fractional quantum Hall regime are in [77–80].

5. Electron heat fluctuations: effects on bigger circuits

We now want to focus on the effect that the quantum heat fluctuations characterising pumped particles have on the thermoelectric quantities in the system where they are injected. We follow [81].

5.1. Model

We consider a two-terminal conductor in the quantum Hall regime. A single particle source, as the Fève's pump [58] or the Leviton pulse [64], is integrated in it, injecting particles in the right lead, while the left reservoir is grounded with chemical potential $\mu = 0$ and it is kept at zero temperature $T = 0$ as sketched in Figure 13. We consider the ideal case of a source pumping one electron (a Leviton for example), or one electron-hole pair (in case of Fève's pump), every pumping period $\mathcal{T}$. The right reservoir is assumed to be a charge and energy conserving voltage probe, characterised by a temperature and a chemical potential. The injection of an electron into the probe will thus slightly modify the potential and the temperature in the probe since each electron emitted from the source carries charge and energy. To conserve in the long time limit, the charge and energy, the probe will develop fluctuations in time of the temperature $T_p(t)$ and the chemical potential $\mu_p(t)$. The chemical potential typically fluctuates around the average value $\bar{\mu}_p$ on the scale of the charge response time τ_{res}, the classical RC-time of the system. The temperature is instead fluctuating around the average value $\bar{T}_p$ on the scale of the dwell-time τ_d of the probe (uncharged fluctuations) [82]. Electrons emitted from the probe propagate towards the left reservoir along the upper edge (Figure 13).

The question we want to answer is: how the wave-packet nature of the injected electrons affects $T_p(t)$ and $\mu_p(t)$ in the probe? Important for the theoretical derivation of the answer is the assumption that both time scales τ_{res} and τ_d are assumed to be much longer than the pumping period $\mathcal{T}$, namely the time between subsequent electron injections into the probe. The other physically relevant time scales are the electron–electron interaction time τ_{e-e} and the inelastic scattering (electron-phonon) time τ_{e-ph}. We work in the hot electron regime $\tau_{e-ph} \gg \tau_d \gg \tau_{e-e}$. In this regime, the electrons thermalise rapidly through electron–electron scattering when entering the probe. The electrons are however assumed to leave the probe before dissipating heat to phonons. As a consequence, as already mentioned, the particle and the total energy currents are conserved by the probe.

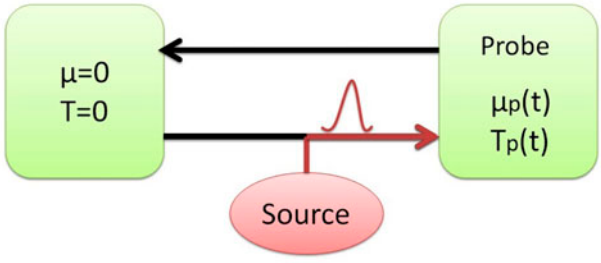

Figure 13. Two-terminal conductor with integrated SPS. The reservoir on the left has chemical potential $\mu = 0$ and it is at zero temperature, $T = 0$. The right lead is a floating probe, conserving energy and charge. Transport takes place along edge states (black arrows). A single electron source pumps electrons propagating towards the probe. This leads to fluctuations in time of the temperature $T_p(t)$ and voltage $V_p(t)$ of the probe.

5.1.1. Basics of probability and full counting statistics

Since it is not possible to perform a measurement able to detect the effect of the injection of a single particle, the simplest measurement that can be done is to detect $\mu = (1/h)\int_0^{t_m} dt\ \mu_p(t)$ and $T = (1/h)\int_0^{t_m} dt\ T_p(t)$, the time averages of the chemical potential and temperature of the probe for a specific run of the experiment of length t_m larger than all the other time scales involved. Due to fluctuations μ and T will vary between different runs, generating a statistical distribution $\mathcal{P}_{t_m}(\mu, T)$. This distribution is related to the distribution $\mathcal{P}_{t_m}(N, E)$ of charge $Q = Ne$ and energy E injected into the probe through the pumping of N electrons during the measurement time t_m.

We first review some basic concepts of probability theory. To fully characterise the probability distribution $\mathcal{P}_{t_m}(N)$ of N countable events (as for example the injections of electrons in the probe) taking place during the measurement time t_m, all cumulants C_n are needed. The cumulants are related to the properties of the probability distribution. For example, the first cumulant C_1 is the mean value of the probability distribution, its variance is instead given by the second cumulant C_2, i.e. the width of the distribution. The so-called skewness is given by $C_3/C_2^{3/2}$ where C_3 is the third cumulant. If the distribution is symmetric around the mean value, the skewness is zero while it is positive if the long tail is at large values of N and negative if it is at small values. The kurtosis excess, indicating how peaked the distribution is and how fat the tails are, is related to the fourth cumulant C_4, namely C_4/C_2^2; it is zero for normal distributions, and so on for the higher cumulants. A pictorial interpretation of the first four cumulants is shown in Figure 14. The cumulants can be defined via the cumulant generating function.

Levitov and co-workers [83–86] developed, in order to calculate the cumulant generating function of $P_{t_m}(N)$, the so-called full counting statistics (FCS), a powerful theoretical scattering approach. Other approaches have been later developed as for example Keldysh-Green's functions techniques [87] or stochastic path integral approach [88,89]. The definition of the cumulant generating function $G(\lambda)$ of the probability distribution $\mathcal{P}_{t_m}(N)$ is given by

$$\mathcal{P}_{t_m}(N) = \int_0^{2\pi} \frac{d\lambda}{2\pi} e^{G(\lambda)} e^{-i\lambda N} \tag{6}$$

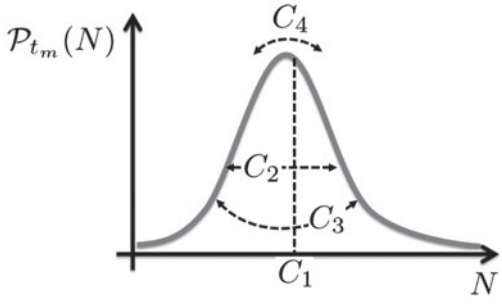

Figure 14. Sketch of the first four cumulants of the probability distribution $\mathcal{P}_{t_m}(N)$. The first cumulant C_1 is the mean value of a distribution. The variance is C_2. The skewness, the asymmetry of the distribution, is given by $C_3/C_2^{3/2}$ while the kurtosis excess, indicating how peaked the distribution is and how fat the tails are, by C_4/C_2^2.

where λ is the so-called counting field. When $\lambda = 0$, as a consequence of the normalisation condition $\sum_N \mathcal{P}_{t_m}(N) = 1$, the cumulant generating function will be zero. Once the cumulant generating function is known all the cumulants can be easily derived as derivatives of it

$$C_j = \left.\frac{\partial^j G(\lambda)}{\partial(i\lambda)^j}\right|_{\lambda=0}. \tag{7}$$

We can extend these concepts to more quantities than charge, as for example energy. The probability distribution for the transmission of N electrons with total energy E during the measurement time t_m, $\mathcal{P}_{t_m}(N, E)$, has cumulant generating function $G(\lambda, \xi)$ given by

$$e^{G(\lambda,\xi)} = \int dE \sum_N e^{i\lambda N + i\xi E} \mathcal{P}_{t_m}(N, E). \tag{8}$$

Going back to our problem the number N of charged particles transmitted to the probe, so the injected charge Q and the energy E brought by them are directly related to the response voltage and temperature originated in the fluctuating probe T_p and μ_p as

$$Q = \nu e \mu_p, \quad E = \nu\left[\frac{\mu_p^2}{2} + \frac{(\pi k_b T_p)^2}{6}\right], \tag{9}$$

where ν is the probe density of states. As said above, we can thus relate $\mathcal{P}_{t_m}(\mu, T)$ to $\mathcal{P}_{t_m}(N, E)$ with a change of variables (see Section 5.3).

In order to have an intuitive understanding of the system properties, we first derive the average values and the zero frequency current correlator, i.e. the first and second cumulants with the Langevin approach. Then we will show the most general results obtained with the stochastic path integral approach to FCS and some examples of specific cases.

5.2. *Langevin approach*

We analyse the temperature and voltage fluctuations in the probe by mean of the Langevin equations (see [90] and references therein). The time-dependent voltage is given by $\mu_p(t) = \bar{\mu}_p + \delta\mu_p(t)$, where μ_p is the time average voltage $\bar{\mu}_p$ and $\delta(t)$ the fluctuating part, and similarly for the temperature of the probe $T_p(t) = \bar{T}_p + \delta T_p(t)$. We will give first the current and the current fluctuations in order to derive $\bar{\mu}_p, \delta\mu_p(t), \bar{T}_p$ and $\delta T_p(t)$. The current and the current fluctuations can be calculated with several approaches. In [81] they have been derived with the scattering matrix approach [7].

5.2.1. *Direct currents*

We define $\bar{I}^{c(e)}(t)$ as the average charge (energy) current. At the probe the average charge current over the measurement time t_m is

$$\bar{I}_p^c = -\frac{e\bar{\mu}_p}{h} + \sigma\frac{e}{\mathcal{T}}. \tag{10}$$

The parameter $\sigma = 0$ for an AC SPS as the Fève's pump and $\sigma = 1$ for a DC SPS as a series of identical Leviton pulses. Due to the charge conserving property of the probe, we have $\bar{I}_p^c = 0$, i.e. no net current into the probe, giving the induced average voltage

$$\bar{\mu}_p = \sigma\frac{h}{\mathcal{T}} = \sigma\hbar\omega. \tag{11}$$

This provides an interesting simple relation between the pumping frequency and the average voltage on the probe. Hohls et al. [91], using a source of the kind realised by Blumenthal et al. [48], exploited this effect to experimentally realise a semiconductor quantised-voltage source in the quantum Hall regime.

Similarly, the average energy current is

$$\bar{I}_c^e = \frac{\langle E\rangle}{\mathcal{T}} - \frac{\bar{\mu}_p^2}{2h} - \frac{k_b^2\pi^2}{6h}\bar{T}_p^2 \tag{12}$$

where $\langle E\rangle$ is the average energy of the particle emitted by the source. In Equation (12), the minus sign in front of the last two terms show that these contributions arise from the probe outgoing particle flux [92]. A discussion of the mesoscopic thermodynamic aspects of these two terms can be found in e.g. [93]. The energy conserving property of the probe, $\bar{I}_p^e = 0$, gives the induced average temperature

$$k_b\bar{T}_p = \sqrt{\frac{6h}{\pi^2\mathcal{T}}[\langle E\rangle - \sigma\hbar\omega]} \tag{13}$$

where we also used the expression for $\bar{\mu}_p$ in Equation (11). We notice that $\bar{T}_p$, defined as in Equation (13), is always positive due to the bathtub principle as argued in [93]. The second term in Equation (13) is the average energy dissipated by a bias voltage at zero temperature.

5.2.2. Current fluctuations

The conservation of charge and energy of the probe in the low-frequency regime imposes that the total fluctuations of the corresponding currents out of the probe are zero as well, $\Delta I_p^c = 0$ and $\Delta I_p^e = 0$. The low-frequency fluctuations

$$\Delta I_p^c = \delta I_p^c + \delta\mu_p \frac{\partial \bar{I}_p^c}{\partial \mu_p} + \delta T_p \frac{\partial \bar{I}_p^c}{\partial T_p} \tag{14}$$

$$\Delta I_p^e = \delta I_p^e + \delta\mu_p \frac{\partial \bar{I}_p^e}{\partial \mu_p} + \delta T_p \frac{\partial \bar{I}_p^e}{\partial T_p} \tag{15}$$

are made up by bare charge and heat fluctuations δI_p^c and δI_p^e, and fluctuations due to the varying temperature and voltage of the probe.

For the voltage fluctuations Equation (14) gives $\Delta I_p^c = 0 = \delta I_p^c - e\delta\mu_p/h$ giving simply that the voltage fluctuations are directly proportional to the bare charge current fluctuations of the probe $\delta\mu_p = h\delta I_p^c/e$. In other words, in order to compensate for the charge fluctuations, the potential of the probe develops fluctuations of the particles emitted from the probe.

The low-frequency voltage correlator then becomes $\langle(\delta\mu_p)^2\rangle = (h^2/e^2)\langle(\delta I_p^c)^2\rangle$. The bare charge current correlator is defined as

$$\langle(\delta I_p^c)^2\rangle \equiv \int_{-\infty}^{\infty} dt \langle I_p^c(t) I_p^c(0)\rangle. \tag{16}$$

The source produces no charge noise and the current correlator simply is $\langle(\delta I_p^c)^2\rangle = e^2 k_b \bar{T}_p/h$. Thus the voltage correlator reads

$$\langle(\delta\mu_p)^2\rangle = h k_b \bar{T}_p. \tag{17}$$

The fluctuation–dissipation type relation in Equation (17) shows that the temperature of an equilibrium electronic system can be probed by charge noise measurements. However, since the average temperature does not contain any information about the heat fluctuations of the source, we cannot infer anything about how the wave-packet width of the source electrons affects the chemical potential and temperature distribution. Turning to the energy current fluctuations we find from Equation (15) that

$$\Delta I_p^e = 0 = \delta I_p^e - \frac{\bar{\mu}_p \delta\mu_p}{h} - \frac{k_b^2\pi^2}{3h}\bar{T}_p \delta T_p. \tag{18}$$

Inserting the result for $\delta\mu_p$ in Equation (18) we can express the temperature fluctuations in terms of bare charge and energy current correlators as

$$k_b \delta T_p = \frac{3h}{\pi^2} \frac{\delta I_p^e - \bar{\mu}_p \delta I_p^c}{k_b \bar{T}_p}. \tag{19}$$

The low-frequency temperature correlations thus become

$$k_b^2\langle(\delta T_p)^2\rangle = \left(\frac{3h}{e\pi^2}\right)^2 \frac{\langle(\delta I_p^e)^2\rangle + (\bar{\mu}_p)^2\langle(\delta I_p^c)^2\rangle - 2e\bar{\mu}_p\langle\delta I_p^e \delta I_p^c\rangle}{(k_b\bar{T}_p)^2}. \tag{20}$$

Importantly, $\langle\delta I_p^e \delta I_p^c\rangle \neq 0$ since the electrons are both energy and charge carriers. From the same results in [94], a study of thermoelectric properties of mesoscopic systems is done in far-from-equilibrium regimes. Evaluating Equation (20), together with the expressions for $\bar{\mu}_p$ and $\bar{T}_p$, we can write

$$k_b^2\langle(\delta T_p)^2\rangle = \frac{3h}{\pi^2}(k_b\bar{T}_p) + \frac{3h}{2\pi^2}\frac{\langle E^2\rangle - \langle E\rangle^2}{\langle E\rangle - \sigma\hbar\omega}. \tag{21}$$

The temperature fluctuations are given by two terms of different nature. The first term is a 'classical' contribution which would be present even if the injected electrons had a well-defined energy. The second term is proportional to the energy fluctuations of the source, resulting from the wave packet, or 'quantum' nature of the emitted electrons.

We also point out that, differently from the correlation between δI_p^e and δI_p^c, there are no correlation between the voltage and the temperature fluctuations, that is $\langle\delta\mu_p\delta T_p\rangle = 0$ since voltage fluctuations are induced by finite temperature not by temperature fluctuations.

5.2.3. Examples: the Fève's pump and the Leviton

To be specific, let's consider the AC source of [58], the Fève's pump, and the DC single particle source, the Lorentzian pulses originating the Levitons [64]. The wave packets [64,67] of both sources, defined at energies E above the Fermi sea, i.e. $E > 0$, have the same analytical expression

$$p(E) = \frac{e^{E/\langle E\rangle}}{\langle E\rangle}. \tag{22}$$

The average particle energy $\langle E\rangle$ in case of a Fève's pump adiabatically driven [67], is given by $\langle E\rangle = \hbar\omega/P_T\Delta$ where P_T is the quantum point contact transparency and Δ is the quantum dot energy spacing, while it is $\langle E\rangle = \hbar/2\tau$ in case of the excitation of a Leviton [64], where τ is the width of the Lorentzian pulse. The Fève's pump does not produce any electrical current, $\bar{\mu}_p = 0$, thus

$$k_b\bar{T}_p = \sqrt{\langle E\rangle\frac{6\hbar\omega}{\pi^2}} \tag{23}$$

and

$$k_b^2\langle(\delta T_p)^2\rangle = \frac{3h}{\pi^2}\sqrt{\langle E\rangle\frac{6\hbar\omega}{\pi^2}} + \frac{3h}{2\pi^2}\langle E\rangle. \tag{24}$$

In case of a Leviton $\bar{\mu}_p = \hbar\omega$ thus

$$k_b\bar{T}_p = \sqrt{\frac{6}{\pi^2}[\langle E\rangle - (\hbar\omega)^2]} \tag{25}$$

and

$$k_b^2\langle(\delta T_p)^2\rangle = \frac{3h}{\pi^2}\sqrt{\frac{6}{\pi^2}[\langle E\rangle - (\hbar\omega)^2]} + \frac{3h}{2\pi^2}\langle E\rangle. \tag{26}$$

Equation (26) shows that the path to suppress the 'classical' fluctuations in case of a Leviton goes via lowering the pumping frequency, not possible instead using the adiabatic Fève's pump.

In conclusion, we find from the Langevin analysis that the wave-packet nature of the electrons affects the temperature fluctuations. Studying the full probability distribution $\mathcal{P}_{t_m}(\mu, T)$ with FCS in Section 5.3, we will show that they do affect voltage higher cumulants as well.

5.3. *Full counting statistics results*

Temperature fluctuations are affected by the energy fluctuations of pumped electrons. However, they are difficult to access experimentally. In order to investigate the appearance of these energy fluctuations in other experimentally accessible quantities, we turn below to an investigation of the higher order cumulants of the joint probability $\mathcal{P}_{t_m}(\mu, T)$.

The joint probability distribution $\mathcal{P}_{t_m}(\mu, T)$ can be defined through its cumulant generating function $G(\chi, \theta)$

$$\mathcal{P}_{t_m}(\mu, T) = \frac{1}{(2\pi)^2} \int d\chi \int d\theta e^{-i\theta T - i\chi\mu + G(\chi,\theta)}, \quad (27)$$

where χ and θ are the counting fields for μ and T, respectively.

We remind briefly the relations between the time scales in the problem. The potential $\mu_p(t)$ fluctuations time scale is given by the RC-time, τ_{res}, while the temperature $T_p(t)$ fluctuations time scale is the dwell-time in the probe, τ_d. We assume also the limit $\tau_{e-e} \ll \tau_{res}, \tau_d \ll \tau_{e-ph}$ and we consider a measurement time such that $t_m \gg \tau_d, \tau_{res} \gg \mathcal{T}$.

5.3.1. *Stochastic path approach to full counting statistics*

We divide our measurement time t_m in small time intervals, $t_m = \sum_n^N t_n$. At each time interval t_n, the energy and the charge in the probe E, Q have a value E_n, Q_n. Working within the framework of the stochastic path integral formalism [88,95], we can then express $G(\chi, \theta)$ as a path integral over all configurations of energy E_n and charge Q_n during the measurement time.

During t_n the extra charge and heat injected into the probe do not change the probe properties appreciably. In other words, the time interval t_n is such that $\mathcal{T} \ll t_n \ll \tau_d, \tau_{res}$. At the time step t_n the net transferred energy E_n and charge Q_n in the probe has a distribution given by the source generating function $h_s(\lambda_n, \xi_n)$ with

$$h_s = \frac{\omega}{2\pi}\left[-ie\sigma\lambda_n + F(\xi_n)\right], \quad (28)$$

where $F(\xi_n)$ is the cumulant generating function of the statistical distribution of the energy emitted by the SPS over the nth time interval t_n and ξ_n the corresponding counting field (see [81]). The probe generating function [83,95,96] $h_p(\lambda_n, \xi_n, E_n, Q_n)$ is given in [95]

$$h_p = \frac{2\mu_n(ei\lambda_n) + k_bT_n(ei\lambda_n)^2 + i\xi_n\left[\pi^2(k_bT_n)^2/3 + \mu_n^2\right]}{(2h)(1-(k_bT_n)i\xi_n)}, \quad (29)$$

where ξ_n and λ_n are counting fields for E_n and Q_n. The chemical potential μ_n and the temperature T_n at the time step n are determined by the total energy and the total charge in the probe at t_n: $\mu_n(E_n, Q_n)$ and $T_n(E_n, Q_n)$ related in Equation (9). At every step t_n, we have the probability distribution $P(Q_n, Q_{n-1}, E_n, E_{n-1})$ given by the generating function $h(\lambda_n, Q_n, \xi_n, E_n) = h_s + h_p$.

The probability $\mathcal{P}_{t_m}(\mu, T)$ can be written taking into account all the possible *paths* in time that μ_n and T_n can take in order to have μ and T at t_m, i.e. satisfying the constraints

$$\mu = \frac{1}{h}\int_0^{t_m} dteV_p(t) = \frac{1}{h}\sum_n^N \mu_n t_n$$
$$T = \frac{1}{h}\int_0^{t_m} dtk_bT(t) = \frac{1}{h}\sum_n^N k_bT_nt_n. \quad (30)$$

Each path has probability $P(Q_0, Q_1, \ldots Q_N, E_0, E_1, \ldots E_N)$ given by the product of conditional probabilities to have Q_n, E_n at time t_n if we had Q_{n-1}, E_{n-1} at time t_{n-1},

$$P(Q_0, Q_1, \ldots Q_N, E_0, E_1, \ldots E_N) = P(Q_N, Q_{N-1}, E_N, E_{N-1}) \ldots P(Q_1, Q_0, E_1, E_0). \quad (31)$$

The full derivation of the cumulant generating function $G(\chi, \theta)$ is cumbersome and rather technical. The interested reader can find more details in [97] together with the explicit expression of $G(\chi, \theta)$.

5.3.2. *Final results*

The low-frequency cumulants of the joint probability distribution $\mathcal{P}_{t_m}(\mu, T)$ are given by successive derivatives of $G(\chi, \theta)$ with respect to χ and θ

$$t_m\langle\delta T_p^n \delta\mu_p^m\rangle = (-ih)^{n+m}k_b^{-n}\frac{\partial_\theta^n\partial_\chi^m G(\chi,\theta)}{(\partial\theta)^n(\partial\chi)^m}|_{\chi,\theta=0}. \quad (32)$$

Expanding $G(\chi, \theta)$ in terms of χ and θ we see that the first two cumulants reproduce the results obtained with the Langevin approach in Section 5.2.

Furthermore, all the even chemical potential cumulants are found to be related to the temperature cumulants as

$$\langle(\delta\mu_p)^{2n}\rangle = (2n-1)!!(k_bh)^n\langle(\delta T_p)^n\rangle. \quad (33)$$

The factorial growth of the cumulants with order n is in agreement with general predictions in [98].

Due to the large number of pumped particles we can evaluate the integral in Equation (27) using the saddle point approximation where χ and θ assume the values χ^*, θ^*. The full distribution $\mathcal{P}_{t_m}(\mu, T)$ is found (to exponential accuracy)

$$\ln\mathcal{P}_{t_m}(\mu, T) = -iT\theta^* + G(0, \theta^*) - \frac{(\mu-\bar{\mu})^2}{2T} \quad (34)$$

where $\bar{\mu} = t_m\bar{\mu}_p/h = \sigma N$. From Equation (34), we immediately learn that the potential μ is characterised by Gaussian fluctuations around the average $\bar{\mu}$, and the width of

the fluctuations is $\sqrt{T}$. Therefore, the marginal potential distribution $\mathcal{P}_{t_m}(\mu) = \int dT \mathcal{P}_{t_m}(\mu, T)$ is symmetric around $\bar{\mu}$, even though $\mathcal{P}_{t_m}(\mu)$ is not Gaussian.

5.3.3. *Marginal distribution $\mathcal{P}_{t_m}(T)$ and specific cases*

The key features of $\mathcal{P}_{t_m}(\mu, T)$ are thus given by the marginal distribution for the temperature $\mathcal{P}_{t_m}(T) = \int d\mu \mathcal{P}_{t_m}(\mu, T)$. The marginal temperature distribution reads

$$\ln \mathcal{P}_{t_m}(T) = -iT\theta^* + G(0, \theta^*). \tag{35}$$

We now illustrate our results for two different cases. We consider a Gaussian spectral distribution

$$p(\epsilon) = \frac{1}{(\sqrt{2\pi}\,\Delta\epsilon)} e^{-\frac{(\epsilon - \langle\epsilon\rangle)^2}{2(\Delta\epsilon)^2}}. \tag{36}$$

Taking the classical limit, $\Delta\epsilon \ll \langle\epsilon\rangle$ we get the simple result

$$\ln \mathcal{P}_{t_m}(T) = -\frac{\pi^2}{6} T \left(1 - \frac{\bar{T}}{T}\right)^2 \tag{37}$$

where we defined similarly to $\bar{\mu}$, $\bar{T} = t_m k_b \bar{T}_p / h$. For small fluctuations $T/\bar{T} - 1 \ll 1$, the distribution is Gaussian, and it is suppressed for $T/\bar{T} \ll 1$ as it should be since $\mathcal{P}_{t_m}(T) \to 0$ when $T \to 0$. When the fluctuations are large $T/\bar{T} \gg 1$, the probability is again suppressed. The plot in Figure 15 shows the log probability. If the width is finite but small $\Delta\epsilon \ll \langle\epsilon\rangle$, the log probability in Equation (37) has a quantum correction given by a multiplying factor $1 + (\Delta\epsilon/\langle\epsilon\rangle)^2 \bar{T}^2 \pi^2/(12TN)$ when $T \sim \bar{T}$.

When instead we consider the distribution of the Fève's pump [67] $p(\epsilon) = (1/\langle\epsilon\rangle) e^{-\epsilon/\langle\epsilon\rangle}$ driven in the adiabatic regime, we find the probability

$$\ln \mathcal{P}_{t_m}(T) = -\frac{\pi^2 \bar{T}}{6} \left(\frac{T}{\bar{T}}(1 - q^*) - \frac{2}{\alpha} \ln \left[\frac{T q^*}{\bar{T}} \right] \right) \tag{38}$$

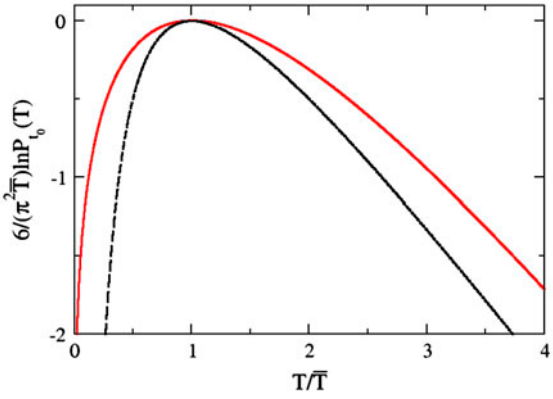

Figure 15. Normalised logarithm of the probability distribution $\mathcal{P}_{t_m}(T)$ as a function of $T/\bar{T}$, with $\bar{T}$ the average value of T in case of the narrow Gaussian wave-packet energy distribution (black dashed) in Equation (37) and in case of the exponential energy distribution with $\alpha = 4$ (red solid) in Equation (38).

where $q^* = (\alpha/2 + \sqrt{\alpha\bar{T}/T + 1 + \alpha^2/4})/(T/\bar{T} + \alpha)$ and $\alpha = \pi\sqrt{\langle\epsilon\rangle/(6\hbar\omega)}$ (Figure 15). When the injection is from a SPS, the probability distribution is wider due to the finite width of the injected wave packet.

6. Conclusion

Single particle sources are now available experimentally and can be realised in several manners as briefly shown in Part I of this review. A lot of effort has been focused on improving the emission accuracy of these devices. This allows the controlled injection of particles in rather complicated circuits. However even in the ideal case of noiseless emission, the injected particles are wave packets with given energy width and thus they are a source of heat fluctuations. It is important to understand the consequences of it when SPSs are coupled to other systems. Quantum heat fluctuations can be detected via electrical potential fluctuations of a probe coupled to the source [81].

Acknowledgements

I acquired the majority of the knowledge about single particle sources and heat fluctuations, presented here, over my PhD studies under the supervision of Peter Samuelsson who I thank also for feedback on a previous version of this manuscript. I thank Liliana Arrachea for reading it. I acknowledge funding by the Excellence Initiative of the German Federal and State Governments and the hospitality of RWTH-Aachen and Universidad de Buenos Aires where this manuscript was partially written.

Notes on contributor

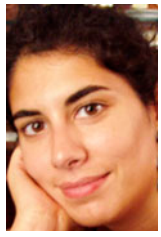

F. Battista is currently a post-doc in the Condensed Matter group at the Physics department of the University of Buenos Aires, Argentina. She did her PhD studies at the Department of Mathematical Physics at Lund University, Sweden. She defended her PhD thesis with the title 'Scattering approach to time-dependent charge and energy transport in mesoscopic conductor' on 25 January 2013. From March 2013 to February 2014 she joined as a post-doc the research group on Dynamics of nanoscale devices at the Institute for Theory of Statistical Physics at RWTH- Aachen, Germany. The focus of her research has been investigating theoretical problems in the field of time dependence and coherence transport in nanoscale systems. The main approaches used are Scattering Matrix Theory, Full Counting Statistics and semiclassical approaches.

References

[1] D.K. Ferry and S. Goodnick, *Transport in Nanostructures*, Cambridge University Press, Cambridge, 1997.

[2] C. Glattli, M. Sanquer, and J. Trân Thanh Vân (eds.), *Quantum Physics at Mesoscopic Scale, Proceedings of the XXXIVth Rencontres de Moriond Series Moriond Workshops*, Les Arcs, EDP Science, 1999.

[3] A. Messiah, *Quantum Mechanics*, Dover, New York, 1999.

[4] D.J. Thouless, *Quantization of particle transport*, Phys. Rev. B 27 (1983), pp. 6083–6087.

[5] M. Büttiker, H. Thomas, and A. Prêtre, *Current partition in multiprobe conductors in the presence of slowly oscillating external potentials*, Z. Phys. B 94 (1994), pp. 133–137.
[6] P.W. Brouwer, *Scattering approach to parametric pumping*, Phys. Rev. B 58 (1998), pp. 10135–10138(R).
[7] Ya. Blanter and M. Büttiker, *Shot noise in mesoscopic conductors*, Phys. Rep. 336 (2000), pp. 1–166.
[8] J.P. Pekola, O.-P. Saira, V.F. Maisi, A. Kemppinen, M. Möttönen, Y.A. Pashkin, and D.V. Averin, *Single-electron current sources: Toward a refined definition of the ampere*, Rev. Mod. Phys. 85 (2013), pp. 1421–1472.
[9] M. Moskalets and M. Büttiker, *Heat production and current noise for single- and double-cavity quantum capacitors*, Phys. Rev. B 80 (2009), pp. 081302–081305(R).
[10] T.T. Heikkilä and Y.V. Nazarov, *Statistics of temperature fluctuations in an electron system out of equilibrium*, Phys. Rev. Lett. 102 (2009), pp. 130605–130608.
[11] M.A. Laakso, T.T. Heikkilä, and Y.V. Nazarov, *Fully overheated single-electron transistor*, Phys. Rev. Lett. 104 (2010), pp. 196805–196808.
[12] R. Sánchez and M. Büttiker, *Detection of single-electron heat transfer statistics*, Europhys. Lett. 100 (2012), pp. 47008–47013.
[13] F. Battista, F. Haupt, and J. Splettstoesser, *Energy and power fluctuations in ac-driven coherent conductors*, preprint (2014), Available at arXiv:1405.4326.
[14] A. Altland, A. De Martino, R. Egger, and B. Narozhny, *Transient fluctuation relations for time-dependent particle transport*, Phys. Rev. B 82 (2010), pp. 115323–115334.
[15] D.V. Averin and J. Pekola, *Violation of the fluctuation-dissipation theorem in time-dependent mesoscopic heat transport*, Phys. Rev. Lett. 104 (2010), pp. 220601–220604; *Statistics of the dissipated energy in driven single-electron transitions*, Europhys. Lett. 96 (2011), pp. 67004–67008.
[16] B. Küng, C. Rössler, M. Beck, M. Marthaler, D.S. Golubev, Y. Utsumi, T. Ihn, and K. Ensslin, *Irreversibility on the level of single-electron tunneling*, Phys. Rev. X. 2 (2012), pp. 011001–011006.
[17] O.-P. Saira, Y. Yoon, T. Tanttu, M. Möttönen, D.V. Averin, and J.P. Pekola, *Test of the Jarzynski and Crooks fluctuation relations in an electronic system*, Phys. Rev. Lett. 109 (2012), pp. 180601–180605.
[18] M. Esposito, U. Harbola, and S. Mukamel, *Nonequilibrium fluctuations, fluctuation theorems, and counting statistics in quantum systems*, Rev. Mod. Phys. 81 (2009), pp. 1665–1702.
[19] G. Haack, M. Moskalets, and M. Büttiker, *Glauber coherence of single-electron sources*, Phys. Rev. B 87 (2013), pp. 201302–201306(R).
[20] A. Mahé, F.D. Parmentier, E. Bocquillon, J.-M. Berroir, D.C. Glattli, T. Kontos, B. Plaçais, G. Féve, A. Cavanna, and Y. Jin, *Current correlations of an on-demand single-electron emitter*, Phys. Rev. B. 82 (2010), pp. 201309–201312(R).
[21] M. Albert, C. Flindt, and M. Büttiker, *Distributions of waiting times of dynamic single-electron emitters*, Phys. Rev. Lett. 107 (2011), pp. 086805–086809.
[22] F.D. Parmentier, E. Bocquillon, J.-M. Berroir, D.C. Glattli, B. Plaçais, G. Fève, M. Albert, C. Flindt, and M. Büttiker, *Current noise spectrum of a single-particle emitter: Theory and experiment*, Phys. Rev. B 85 (2012), pp. 165438–165452.
[23] R.-P. Riwar and J. Splettstoesser, *Charge and spin pumping through a double quantum dot*, Phys. Rev. B 82 (2010), pp. 205308–205321.
[24] B.D. Josephson, *Possible new effects in superconductive-tunnelling*, Phys. Lett. 1 (1962), pp. 251–253.
[25] K. von Klitzing, G. Dorda, and M. Pepper, *New method for high-accuracy determination of the fine-structure constant based on quantized hall resistance*, Phys. Rev. Lett. 45 (1980), pp. 494–497.
[26] P. Samuelsson, E.V. Sukhorukov, and M. Büttiker, *Two-particle Aharonov-Bohm effect and entanglement in the electronic Hanbury Brown-Twiss setup*, Phys. Rev. Lett. 92 (2004), pp. 026805–026808; P. Samuelsson, I. Neder, and M. Büttiker, *Reduced and projected two-particle entanglement at finite temperatures*, Phys. Rev. Lett. 102 (2009), pp. 106804–106807.
[27] R.A. Webb, S. Washburn, C.P. Umbach, and R.B. Laibowitz, *Observation of h/e Aharonov-Bohm oscillations in normal-metal rings*, Phys. Rev. Lett. 54 (1985), pp. 2696–2699.
[28] Y. Ji, Y. Chung, D. Sprinzak, M. Heiblum, D. Mahalu, and H. Shtrikman, *An electronic Mach-Zehnder interferometer*, Nature 422 (2003), pp. 415–418; I. Neder, M. Heiblum, Y. Levinson, D. Mahalu, and V. Umansky, *Unexpected behavior in a two-path electron interferometer*, Phys. Rev. Lett. 96 (2006), pp. 016804–016807; L.V. Litvin, H. Tranitz, W. Wegscheider, and C. Strunk, *Decoherence and single electron charging in an electronic Mach-Zehnder interferometer*, Phys. Rev. B 75 (2007), pp. 033315–033318; P. Roulleau, F. Portier, P. Roche, A. Cavanna, G. Faini, U. Gennser, and D. Mailly, *Direct measurement of the coherence length of edge states in the integer quantum hall regime*, Phys. Rev. Lett. 100 (2008), pp. 126802–126805; E. Bieri, M. Weiss, O. Goktas, M. Hauser, S. Csonka, S. Oberholzer, and C. Schonenberger, *Finite-bias visibility dependence in an electronic Mach-Zehnder interferometer*, Phys. Rev. B 79 (2009), pp. 245324–245329.
[29] E. Bocquillon, F.D. Parmentier, C. Grenier, J.-M. Berroir, P. Degiovanni, D.C. Glattli, B. Plaçais, A. Cavanna, Y. Jin, and G. Fève, *Electron quantum optics: Partitioning electrons one by one*, Phys. Rev. Lett. 108 (2012), pp. 196803–196807.
[30] M. Büttiker, *Absence of backscattering in the quantum Hall effect in multiprobe conductors*, Phys. Rev. B 38 (1988), pp. 9375–9389.
[31] C. Grenier, R. Hervé, G. Fève, and P. Degiovanni, *Pascal Degiovanni*, *Electron quantum optics in quantum hall edge channels*, Mod. Phys. Lett. B 25 (2011), pp. 1053–1073.
[32] L.J. Geerlings, V.F. Anderegg, P.A.M. Holweg, and J.E. Mooij, *Frequency-locked turnstile device for single electrons*, Phys. Rev. Lett. 64 (1990), pp. 2691–2694.
[33] H. Pothier, P. Lafarge, C. Urbina, D. Esteve, and M.H. Devoret, *Single-electron pump based on charging effects*, Europhys. Lett. 17 (1992), pp. 249–254.
[34] B. Camarota, H. Scherer, M.V. Keller, S.V. Lotkhov, G.-D. Willenberg, and F.J. Ahlers, *Electron counting capacitance standard with an improved five-junction R-pump*, Metrologia 49 (2012), pp. 8–23.
[35] L.P. Kouwenhoven, A.T. Johnson, N.C. van der Vaart, C.J.P.M. Harmans, and C.T. Foxon, *Quantized current in a quantum-dot turnstile using oscillating tunnel barriers*, Phys. Rev. Lett. 67 (1991), pp. 1626–1629.
[36] N.M. Zimmerman, E. Hourdakis, Y. Ono, A. Fujiwara, and Y. Takahashi, *Error mechanisms and rates in tunable-barrier single-electron turnstiles and charge-coupled devices*, J. Appl. Phys. 96 (2004), pp. 5254–5266.
[37] J.M. Shilton, V.I. Talyanskii, M. Pepper, D.A. Ritchie, J.E.F. Frost, C.J.B. Ford, C.G. Smith, and G.A.C. Jones, *High-frequency single-electron transport in aquasi-one-*

dimensional GaAs channel induced by surface acoustic waves, J. Phys.: Condens. Matter 8 (1996), pp. L531–539.

[38] A.M. Robinson and C.H.W. Barnes, *Classical dynamics of electrons in quantized-acoustoelectric-current devices*, Phys. Rev. B 63 (2001), pp. 165418–165429.

[39] P.A. Maksym, *Quantized electron transport through a time-dependent potential barrier*, Phys. Rev. B 61 (2000), pp. 4727–4730.

[40] K. Flensberg, Q. Niu, and M. Pustilnik, *Nonadiabaticity and single-electron transport driven by surface acoustic waves*, Phys. Rev. B 60 (1999), pp. 16291–16294(R).

[41] G.R. Aizin, G. Gumbs, and M. Pepper, *Screening of the surface-acoustic-wave potential by a metal gate and the quantization of the acoustoelectric current in a narrow channel*, Phys. Rev. B 58 (1998), pp. 10589–10596.

[42] G. Gumbs, G.R. Aizin, and M. Pepper, *Coulomb interaction of two electrons in the quantum dot formed by the surface acoustic wave in a narrow channel*, Phys. Rev. B 60 (1999), pp. 13954–13957(R).

[43] R.P.G. McNeil, M. Kataoka, C.J.B. Ford, C.H.W. Barnes, D. Anderson, G.A.C. Jones, I. Farrer, and D.A. Ritchie, *On-demand single-electron transfer between distant quantum dots*, Nature 477 (2011), pp. 439–442.

[44] S. Hermelin, S. Takada, M. Yamamoto, S. Tarucha, A.D. Wieck, L. Saminadayar, C. Bäuerle, and T. Meunier, *Electrons surfing on a sound wave as a platform for quantum optics with flying electrons*, Nature 477 (2011), pp. 435–438.

[45] J.P. Pekola, J.J. Vartiainen, M. Möttönen, O.-P. Saira, M. Meschke, and D.V. Averin, *Hybrid single-electron transistor as a source of quantized electric current*, Nature Phys. 4 (2008), pp. 120–124.

[46] J.P. Pekola, F. Maisi, S. Kafanov, N. Chekurov, A. Kempinen, Y.A. Pashkin, O.-P. Saira, M. Möttönen, and J.S. Tsai, *Environment-assisted tunneling as an origin of the dynes density of states*, Phys. Rev. Lett. 105 (2010), pp. 026803–026806.

[47] V.F. Maisi, Y.A. Pashkin, S. Kafanov, J.S. Tsai, and J.P. Pekola, *Parallel pumping of electrons*, New J. Phys. 11 (2009), pp. 113057–113062.

[48] M.D. Blumenthal, B. Kaestner, L. Li, S. Giblin, T.J.B.M. Janssen, M. Pepper, D. Anderson, G. Jones, and D.A. Ritchie, *Gigahertz quantized charge pumping*, Nature Phys. 3 (2007), pp. 343–347.

[49] B. Kaestner, V. Kashcheyevs, S. Amakawa, M.D. Blumenthal, L. Li, T.J.B.M. Janssen, G. Heinz, K. Pierz, T. Weimann, U. Siegner, and H.W. Schumacher, *Single-parameter nonadiabatic quantized charge pumping*, Phys. Rev. B 77 (2008), pp. 153301–153304.

[50] A. Fujiwara, K. Nishiguchi, and Y. Ono, *Nanoampere charge pump by single-electron ratchet using silicon nanowire metal-oxide-semiconductor field-effect transistor*, Appl. Phys. Lett. 92 (2008), pp. 042102–042102-3.

[51] B. Kaestner, C. Leicht, V. Kashcheyevs, K. Pierz, U. Siegner, and H.W. Schumacher, *Single-parameter quantized charge pumping in high magnetic fields*, Appl. Phys. Lett. 94 (2009), pp. 012106–012109.

[52] S.J. Wright, M.D. Blumenthal, G. Gumbs, A.L. Thorn, M. Pepper, T.J.B.M. Janssen, S.N. Holmes, D. Anderson, G.A.C. Jones, C.A. Nicoll, and D.A. Ritchie, *Enhanced current quantization in high-frequency electron pumps in a perpendicular magnetic field*, Phys. Rev. B 78 (2008), pp. 233311–23334.

[53] S. Giblin, M. Kataoka, J.D. Fletcher, P. See, T.J.B.M. Janssen, J.P. Griffiths, G.A.C. Jones, I. Farrer, and D.A. Ritchie, *Towards a quantum representation of the ampere using single electron pumps*, Nat. Commun. 3 (2012), pp. 930–937.

[54] T. Shinada, S. Okamoto, T. Kobayashi, and I. Ohdomari, *Enhancing semiconductor device performance using ordered dopant arrays*, Nature 437 (2005), pp. 1128–1131.

[55] M. Tabe, D. Moraru, M. Ligowski, M. Anwar, R. Jablonski, Y. Ono, and T. Mizuno, *Single-electron transport through single dopants in a dopant-rich environment*, Phys. Rev. Lett. 105 (2010), pp. 016803–016806.

[56] G.P. Lansbergen, Y. Ono, and A. Fujiwara, *Donor-based single electron pumps with tunable donor binding energy*, Nano Lett. 12 (2012), pp. 763–768.

[57] B. Roche, R.-P. Riwar, B. Voisin, E. Dupont-Ferrier, R. Wacquez, M. Vinet, M. Sanquer, J. Splettstoesser, and X. Jehl, *A two-atom electron pump*, Nature Commun. 4 (2013), pp. 1581–1585.

[58] G. Fève, A. Mahé, J.-M. Berroir, T. Kontos, B. Plaçais, D.C. Glattli, A. Cavanna, B. Etienne, and Y. Jin, *An on-demand coherent single-electron source*, Science 316 (2007), pp. 1169–1172.

[59] F. Battista and P. Samuelsson, *Proposal for nonlocal electron-hole turnstile in the quantum Hall regime*, Phys. Rev. B 83 (2011), pp. 125324–125328.

[60] M. Moskalets, P. Samuelsson, and M. Büttiker, *Quantized dynamics of a coherent capacitor*, Phys. Rev. Lett. 100 (2008), pp. 086601–086604.

[61] J. Keeling, A.V. Shytov, and L.S. Levitov, *Coherent particle transfer in an on-demand single-electron source*, Phys. Rev. Lett. 101 (2008), pp. 196404–196407.

[62] T. Jonckheere, T. Stoll, J. Rech, and Th. Martin, *Real-time simulation of finite-frequency noise from a single-electron emitter*, Phys. Rev. B 85 (2012), pp. 045321–045329.

[63] S. Ol'khovskaya, J. Splettstoesser, M. Moskalets, and M. Büttiker, *Shot noise of a mesoscopic two-particle collider*, Phys. Rev. Lett. 101 (2008), pp. 166802–166805.

[64] J. Keeling, I. Klich, and L.S. Levitov, *Minimal excitation states of electrons in one-dimensional wires*, Phys. Rev. Lett. 97 (2006), pp. 116403–116406.

[65] J. Dubois, J. Thibaut, C. Grenier, P. Degiovanni, P. Roulleau, and D.C. Glattli, *Integer and fractional charge Lorentzian voltage pulses analyzed in the framework of photon-assisted shot noise*, Phys. Rev. B 88 (2013), pp. 085301–085315.

[66] J. Dubois, T. Jullien, F. Portier, P. Roche, A. Cavanna, Y. Jin, W. Wegscheider, P. Roulleau, and D.C. Glattli, *Minimal-excitation states for electron quantum optics using levitons*, Nature 502 (2013), pp. 659–663.

[67] J. Keeling, A.V. Shytov, and L.S. Levitov, *Coherent particle transfer in an on-demand single-electron source*, Phys. Rev. Lett. 101 (2008), pp. 196404–196407.

[68] F. Battista and P. Samuelsson, *Spectral distribution and wave function of electrons emitted from a single-particle source in the quantum hall regime*, Phys. Rev. B 85 (2012), pp. 075428–075438.

[69] J.D. Fletcher, P. See, H. Howe, M. Pepper, S.P. Giblin, J.P. Griffiths, G.A.C. Jones, I. Farrer, D.A. Ritchie, T.J.B.M. Janssen, and M. Kataoka, *Clock-controlled emission of single-electron wave packets in a solid-state circuit*, Phys. Rev. Lett. 111 (2013), pp. 216807–216811.

[70] D. Ferraro, A. Feller, A. Ghibaudo, E. Thibierge, E. Bocquillon, G. Fève, C. Grenier, and P. Degiovanni, *Wigner function approach to single electron coherence in quantum hall edge channels*, Phys. Rev. B 88 (2013), pp. 205303–205319.

[71] C. Altimiras, H. le Sueur, U. Gennser, A. Cavanna, D. Mailly, and F. Pierre, *Non-equilibrium edge-channel*

spectroscopy in the integer quantum Hall regime, Nature Phys. 6 (2009), pp. 34–39.
[72] H. le Sueur, C. Altimiras, U. Gennser, A. Cavanna, D. Mailly, and F. Pierre, *Energy relaxation in the integer quantum hall regime*, Phys. Rev. Lett. 105 (2010), pp. 056803–056806.
[73] C. Altimiras, H. le Sueur, U. Gennser, A. Cavanna, D. Mailly, and F. Pierre,*Tuning energy relaxation along quantum hall channels*, Phys. Rev. Lett. 105 (2010), pp. 226804–226807.
[74] C. Neuenhahn and F. Marquardt, *Universal dephasing in a Chiral 1D interacting Fermion System*, Phys. Rev. Lett. 102 (2009), pp. 046806–046809.
[75] P. Degiovanni, C. Grenier, and G. Fève, *Decoherence and relaxation of single-electron excitations in quantum Hall edge channels*, Phys. Rev. B 80 (2009), pp. 241307–241310.
[76] A.M. Lunde, S.E. Nigg, and M. Buttiker, *Interaction-induced edge channel equilibration*, Phys. Rev. B 81 (2010), pp. 041311–041314(R).
[77] G. Granger, J.P. Eisenstein, and J.L. Reno, *Observation of chiral heat transport in the quantum hall regime*, Phys. Rev. Lett. 102 (2009), pp. 086803–086806.
[78] V. Venkatachalam, S. Hart, L. Pfeiffer, K. West, and A. Yacoby, *Local thermometry of neutral modes on the quantum Hall edge*, Nature Phys. 8 (2012), pp. 676–681.
[79] C. Altimiras, H. le Sueur, U. Gennser, A. Anthore, A. Cavanna, D. Mailly, and F. Pierre, *Chargeless heat transport in the fractional quantum hall regime*, Phys. Rev. Lett. 109 (2012), pp. 026803–026807.
[80] S. Jezouin, F.D. Parmentier, A. Anthore, U. Gennser, A. Cavanna, Y. Jin, and F. Pierre, *Quantum limit of heat flow across a single electronic channel*, Science 342 (2013), pp. 601–604.
[81] F. Battista, M. Albert, M. Moskalets, and P. Samuelsson, *Quantum heat fluctuations of single-particle sources*, Phys. Rev. Lett. 110 (2013), pp. 126602–126606.
[82] K.E. Nagaev, S. Pilgram, and M. Büttiker, *Frequency scales for current statistics of mesoscopic conductors*, Phys. Rev. Lett. 92 (2004), pp. 176804–176807.
[83] L.S. Levitov and G.B. Lesovik, *Charge distribution in quantum shot noise*, JETP Lett. 58 (1993), pp. 230–235.
[84] D.A. Ivanov and L.S. Levitov, *Statistics of charge fluctuations in quantum transport in an alternating field*, JETP Lett. 58 (1993), pp. 461–468.
[85] L.S. Levitov, H.-W. Lee, and G.B. Lesovik, *Electron counting statistics and coherent states of electric current*, J. Math. Phys. 37 (1996), pp. 4845–4387.
[86] D.A. Ivanov, H.-W. Lee, and L.S. Levitov, *Coherent states of alternating current*, Phys. Rev. B 56 (1997), pp. 6839–6850.
[87] Y.V. Nazarov (ed.), *Quantum Noise in Mesoscopic Physics*, Vol. 97 of *NATO ASI Series II*, Kluwer, Dordrecht, 2003.
[88] S. Pilgram, A.N. Jordan, E.V. Sukhorukov, and M. Büttiker, *Stochastic path integral formulation of full counting statistics*, Phys. Rev. Lett. 90 (2003), pp. 206801–206804.
[89] A.N. Jordan, E.V. Sukhorukov, and S. Pilgram, *Fluctuation statistics in networks: A stochastic path integral approach*, J. Math. Phys. 45 (2004), pp. 4386–4408.
[90] H. Förster, P. Samuelsson, and M. Büttiker, *Current-voltage correlations in interferometers*, New J. Phys. 9 (2007), pp. 117–138.
[91] F. Hohls, A.C. Welker, Ch Leicht, L. Fricke, B. Kaestner, P. Mirovsky, A. Müller, K. Pierz, U. Siegner, and H.W. Schumacher, *Semiconductor quantized voltage source*, Phys. Rev. Lett. 109 (2012), pp. 056802–056806.
[92] L.G.C. Rego and G. Kirczenow, *Fractional exclusion statistics and the universal quantum of thermal conductance: A unifying approach*, Phys. Rev. B 59 (1999), pp. 13080–13086.
[93] J.E. Avron, A. Elgart, G.M. Graf, and L. Sadun, *Optimal quantum pumps*, Phys. Rev. Lett. 87 (2001), pp. 236601–236604.
[94] A. Crépieux and F. Michelini, *Mixed, charge and heat noises in thermoelectric nanosystems*, preprint (2014). Available at arXiv:1403.8035.
[95] S. Pilgram, *Electron-electron scattering effects on the full counting statistics of mesoscopic conductors*, Phys. Rev. B 69 (2004), pp. 115315–115322.
[96] M. Kindermann and S. Pilgram, *Statistics of heat transfer in mesoscopic circuits*, Phys. Rev. B 69 (2004), pp. 155334–155341.
[97] F. Battista, M. Albert,, M. Moskalets, and P. Samuelsson, *Statistics of temperature and potential fluctuations induced by coherent single particle sources*, in *Proceedings of the 22nd International Conference on Noise and Fluctuations (ICNF)*, 24–28 June 2013, Montpellier, France, IEEE, 2013.
[98] C. Flindt, C. Fricke, F. Hohls, T. Novotný, K. Netočný, T. Brandes, and R.J. Haug, *Universal oscillations in counting statistics*, Proc. Natl. Acad. Sci. USA 106 (2009), pp. 10116–10119.